High-temperature phase chemistry of the system Gd–Pd–O

2002 Sci. Technol. Adv. Mater. 3 75

(http://iopscience.iop.org/1468-6996/3/2/A03)

ELSEVIER

Science and Technology of Advanced Materials 3 (2002) 75–84

SCIENCE AND TECHNOLOGY OF ADVANCED MATERIALS

www.elsevier.com/locate/stam

High-temperature phase chemistry of the system Gd–Pd–O

K. Thomas Jacob[a,*], Kay Thi Lwin[a], Yoshio Waseda[b]

[a]*Department of Metallurgy, Indian Institute of Science, Bangalore 560012, India*
[b]*Institute for Multidisciplinary Research on Advanced Materials, Tohoku University, Sendai 980-8577, Japan*

Received 2 July 2001; revised 5 September 2001; accepted 10 October 2001

Abstract

An isothermal section of the phase diagram for the system Gd–Pd–O at 1223 K has been established by equilibration of samples and phase identification after quenching by optical and scanning electron microscopy, X-ray powder diffraction, and energy dispersive spectroscopy. Three ternary oxides Gd_4PdO_7, Gd_2PdO_4 and $Gd_2Pd_2O_5$ were identified. Liquid alloys, the four inter-metallic compounds and Pd-rich solid solution were found to be in equilibrium with Gd_2O_3.

Based on the phase relations, four solid-state cells were designed to measure the Gibbs energies of formation of the three ternary oxides in the temperature range from 920 to 1320 K. Although three cells are sufficient to obtain the properties of the three compounds, the fourth cell was deployed to cross check the data. An advanced version of the solid-state cell incorporating a buffer electrode with yttria-stabilized zirconia solid electrolyte and pure oxygen gas at a pressure of 0.1 MPa as the reference electrode was used for high-temperature thermodynamic measurements. The standard Gibbs energy of formation of the inter-oxide compounds from their component binary oxides can be represented by the following equations:

$$Gd_4PdO_7(s) : \Delta_{f(ox)}G^0/\text{J mol}^{-1} = -25,030 + 0.33T \quad (\pm 140), \qquad Gd_2PdO_4(s) : \Delta_{f(ox)}G^0/\text{J mol}^{-1} = -25,350 + 0.84T \quad (\pm 135),$$

$$Gd_2Pd_2O_5(s) : \Delta_{f(ox)}G^0/\text{J mol}^{-1} = -48,700 + 0.38T \quad (\pm 270)$$

Based on the thermodynamic information, isothermal chemical potential diagrams and isobaric phase diagrams for the system Gd–Pd–O are developed.

Keywords: Phase diagram; Gibbs energy; Enthalpy; Entropy; Gd_4PdO_7; Gd_2PdO_4; $Gd_2Pd_2O_5$

1. Introduction

As a part of systematic studies on phase equilibria and thermodynamic properties of compounds in the ternary systems Re–X–O, where Re is a rare earth element and X is a metal from the platinum group, measurements have been made on the system Gd–Pd–O at high-temperatures. Some of the ternary oxides of this group have potential application in catalysis and electrochemistry. The compound Gd_4PdO_7 exhibits three-way catalytic behavior for automobile exhaust clean-up, simultaneously aiding the oxidation of CO and the hydrocarbons and the reduction of NO [1]. To understand the behavior of the catalysts, it is useful to have information on the thermodynamic stability domain of the compound. Quantitative information on the stability of the ternary oxides is also useful for assessing the interaction of Pt-group metals with ceramic compounds containing rare earth elements under different environments. Furthermore, the thermodynamic data are beneficial for the design of processes for the recovery of rare earth and precious metals from scrap. Phase diagrams of higher order systems containing these elements can be readily computed from thermodynamic data on binary and ternary compounds.

Two stable ternary compounds, Gd_2PdO_4 and $Gd_2Pd_2O_5$, were reported in the system Gd–Pd–O by McDaniel and Schneider [2]. Recently, Andersson et al. [3] have shown that Ln_4PdO_7 compounds for Ln = La, Nd, Sm, Eu, and Gd can be indexed on a triclinic unit cell (space group $P\bar{1}$). The chains of PdO_4 squares are staggered, except in the case of La_4PdO_7. The lattice parameters of Gd_4PdO_7 are $a = 1.5795$ nm, $b = 0.71142$ nm, $c = 0.67853$ nm, $\alpha = 95.723°$, $\beta = 131.241°$, and $\gamma = 122.771°$. The compound $Gd_2Pd_2O_5$ decomposes to Gd_4PdO_7, Pd and O_2 in air at ~1298 K, and Gd_2PdO_4 decomposes to $Gd_2Pd_2O_5$ and Gd_4PdO_7 at ~1278 K, according to McDaniel and Schneider [2].

* Corresponding author. Tel.: +91-80-309-2494; fax: +91-80-360-0683.
E-mail address: katob@metalrg.iisc.ernet.in (K.T. Jacob).

1468-6996/02/$ - see front matter
PII: S1468-6996(01)00152-8

In this study, phase equilibria involving the oxide phases were first determined at 1223 K by isothermal equilibration and phase analysis of quenched samples. Based on the phase diagram, solid-state cells were designed to measure the Gibbs energies of formation of the ternary oxides. In general, the electrochemical method has been found simpler and superior to other techniques for the determination of Gibbs energies of formation of oxides [4]. Yttria-stabilized zirconia (YSZ) was used as the solid electrolyte and pure oxygen at a pressure of 0.1 MPa as the non-polarizable reference electrode. Errors in electrochemical measurements often arise from polarization of the electrodes, especially when they contain more than two phases. Because of the difference in the chemical potential of the mobile species between the reference and working electrodes of such cells, there is always a small flux through the electrolyte separating them, even in the absence of physical porosity [5]. The electrochemical permeability is caused by coupled transport of mobile ions and holes (or electrons) in the solid electrolyte under the chemical potential gradient. Used in this study was a buffer electrode, which absorbed the flux and prevented polarization of the measuring electrode. This new special feature and the use of the primary reference standard for oxygen chemical potential allowed the generation of accurate data on the ternary oxides.

2. Experimental

2.1. Materials

Reactive forms of Gd_2O_3 and PdO were used as the starting materials for the synthesis of the ternary oxides. The reactive binary oxides were prepared by the decomposition of the respective nitrates at reduced pressure (10 Pa); $Gd(NO_3)_3{\cdot}6H_2O$ at 1073 K and $Pd(NO_3)_2$ at 723 K. The inter-oxide compounds Gd_4PdO_7 and $Gd_2Pd_2O_5$ were prepared by heating pellets containing Gd_2O_3 and PdO in the appropriate ratio at 1300 K in dry oxygen for six days, with regrinding and recompaction at intervals of two days in a glove box. The pellets were then homogenized at 1350 K in pure dry oxygen for 12 h. The pellets, prepared from an intimate mixture of the components by compaction at 150 MPa using steel die, were contained in calcia crucibles and supported on sacrificial pellets of the same composition. The compound Gd_2PdO_4 was made by direct reaction of Gd_2O_3 and PdO at 1223 K in pure oxygen for two days. The pellet was ground to fine powder and then compacted again for further heat treatment for four days. The intermetallics (GdPd, Gd_3Pd_4, $GdPd_2$ and $GdPd_3$) were prepared by the powder metallurgy route. The powders of the two pure metals, each of 99.9% purity, were mixed in the stoichiometric ratio, compacted at 150 MPa, placed in a closed Mo crucible, and heat-treated at 1275 K for four days in evacuated quartz ampoules. Placing titanium foil around the sample prevented oxidation during subsequent annealing in prepurified argon gas at 1350 K. The formation of inter-metallics and inter-oxide compounds was confirmed by XRPD. The lattice parameters of the inter-metallics and oxides were in good accord with values reported in the literature [3,6]. YSZ tubes and crucibles were obtained from Zircoa Corporation.

2.2. Determination of the phase diagram

The phase relations were explored by equilibrating mixtures of metals or inter-metallics with the different oxides at 1223 K, followed by quenching in liquid nitrogen or chilled mercury and phase identification. Thus, 16 compositions were equilibrated for periods up to 18 days; one along the binary Gd–O, and the rest inside the ternary. During this period, twice the samples were quenched, ground to −325 mesh, and repelletized for further heat treatment. The phase compositions of the samples were unaltered by further heating. The average composition of the samples studied is shown by cross marks on the Gibbs triangle in Fig. 1.

Two arrangements were used for equilibrating samples at high-temperature. Several mixtures containing Gd_2O_3, PdO, and the inter-oxide compounds were equilibrated in pure oxygen at a pressure of 0.1 MPa, using an apparatus described earlier [7]. The samples were held in calcia crucibles, and kept on sacrificial disks of the same composition. The mass of each sample pellet was determined before and after equilibration. Sample pellets containing either pure metal or alloy were contained in closed Mo crucibles, which were sealed in evacuated quartz ampoules. To minimize physical contact between the pellet and the Mo crucible, the pellet was placed on a disc containing only the oxides. This precaution was taken to avoid contamination of

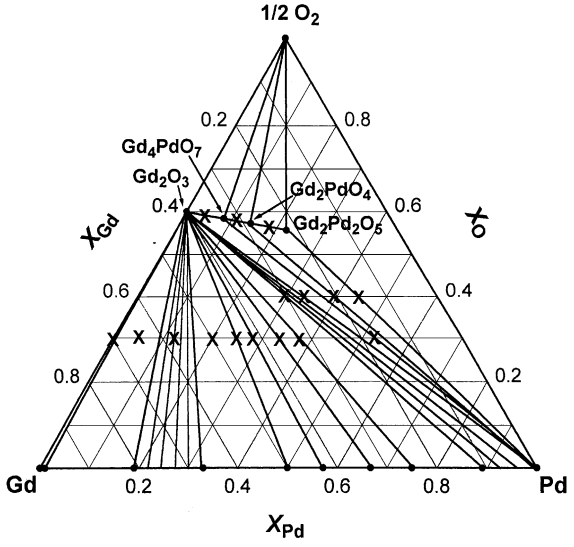

Fig. 1. Isothermal section of the phase diagram for the system Gd–Pd–O at 1223 K. The average composition of the samples examined in this study is shown by the symbol ×.

the samples by molybdenum. In many cases, samples of the same overall composition were made, using different starting materials. Optical and scanning electron microscopy, EDS, and XRPD identified phases present in the quenched samples.

2.3. Measurement of Gibbs energies of formation of ternary oxides

The reversible emf of the following solid-state cells were measured as a function of temperature

$$\text{Pt, Pd} + \text{Gd}_4\text{PdO}_7 + \text{Gd}_2\text{O}_3//(\text{Y}_2\text{O}_3)\text{ZrO}_2//\text{O}_2(0.1\ \text{MPa}), \text{Pt} \quad \text{Cell 1}$$

$$\text{Pt, Pd} + \text{Gd}_2\text{PdO}_4 + \text{Gd}_4\text{PdO}_7//(\text{Y}_2\text{O}_3)\text{ZrO}_2//\text{O}_2(0.1\ \text{MPa}), \text{Pt} \quad \text{Cell 2}$$

$$\text{Pt, Pd} + \text{Gd}_2\text{Pd}_2\text{O}_5 + \text{Gd}_2\text{PdO}_4//(\text{Y}_2\text{O}_3)\text{ZrO}_2//\text{O}_2(0.1\ \text{MPa}), \text{Pt} \quad \text{Cell 3}$$

The cells were designed based on the phase relations established at 1223 K. During the course of the emf studies, it was found that the compound Gd_2PdO_4 decomposed above 1280 K. A new three-phase region involving Pd, Gd_4PdO_7 and $Gd_2Pd_2O_5$, thus came into existence at $T \geq 1280$ K. Hence, the emf of a fourth cell:

$$\text{Pt, Pd} + \text{Gd}_2\text{Pd}_2\text{O}_5 + \text{Gd}_4\text{PdO}_7//(\text{Y}_2\text{O}_3)\text{ZrO}_2//\text{O}_2(0.1\ \text{MPa}), \text{Pt} \quad \text{Cell 4}$$

was measured from 1280 to 1320 K.

Two experiments were conducted on each cell. All the cells are written such that the right hand electrodes are positive. (Y_2O_3) ZrO_2 is an oxygen ion conductor with ionic transport number greater than 0.99 at the temperatures and oxygen partial pressures encountered in this study [4]. However, the presence of trace hole conduction in the electrolyte gives rise to a small electrochemical flux of oxygen from the reference electrode on the right side to the working electrodes on the left side of each cell [5]. The electrochemical permeability is caused by the coupled transport of oxygen ions and holes in the solid electrolyte under the oxygen potential gradient. Only opposing it with an external dc voltage, exactly equivalent to the oxygen chemical potential difference, can stop this flow of oxygen [8].

The electrochemical flux of oxygen would have caused polarization of the multiphase solid electrodes. The chemical potential of oxygen in the microsystem near the solid electrode/electrolyte interface would have been altered because of the semipermeability of the electrolyte to oxygen. A buffer electrode, introduced between reference and working electrodes was designed to act as a sink for the oxygen flux and prevent the flux from reaching the working electrode. The buffer electrode was maintained at an oxygen chemical potential close to that of the working electrode. Since there was no significant difference between the chemical potentials of buffer and working electrodes, driving force for transport of oxygen through the zirconia tube separating these electrodes did not exist. The working electrode therefore remained unpolarized. Pure oxygen gas at a pressure of 0.1 MPa, flowing over a platinized surface of zirconia, constituted the primary reference standard for oxygen chemical potential and formed a non-polarizable electrode. Thus, the three electrode design of the cell prevented error in emf caused by polarization of the working electrode. Measuring separately the emf between the three electrodes, two at a time, assessed the magnitude of the polarization effect. Transport of oxygen between the electrodes through the gas phase was prevented by physical isolation of the gas phase over the three electrodes.

The cell design used for high-temperature emf measurements is shown in Fig. 2. It consisted of three distinct compartments, separated by two impervious YSZ tubes and a YSZ crucible. The cell can be represented schematically as follows:

Working Electrode O_2 (P'_{O2}), Pt/Pd	$(Y_2O_3)ZrO_2$ No flux	Buffer Electrode O_2 (P''_{O2}), Pt/Pd $P''_{O2} \approx P'_{O2}$	$(Y_2O_3)ZrO_2$ ← O^{2-}	Reference Electrode O_2 (0.1 MPa), Pt

The working and reference electrodes were contained inside separate zirconia tubes. The cell emf measured between the working and reference electrodes was determined only by the oxygen chemical potential at these electrodes and was not affected by the gradient of chemical potential through the connecting chain consisting of the solid electrolyte segments and the buffer electrode. Construction of the high-temperature galvanic cell was rendered more difficult by the introduction of the buffer electrode. Moreover, in some of the cells used in this study, the partial pressure of oxygen at the working electrode was quite appreciable, especially at the higher

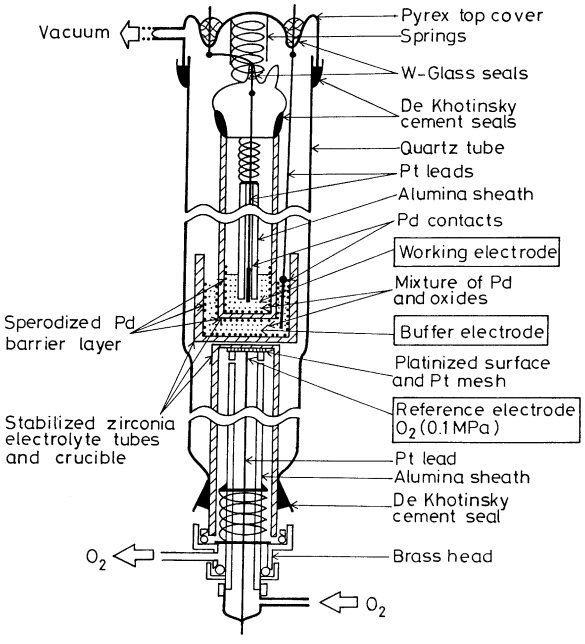

Fig. 2. A schematic diagram of the new apparatus for high-temperature emf measurements, with a buffer electrode interspersed between reference and working electrodes.

temperatures. Therefore, the static sealed design used by Charette and Flengas [9] was found more appropriate than other designs that employ either dynamic vacuum or inert gas flow over the electrodes [4,10].

The working electrode consisted of a mixture of Pd + Gd_4PdO_7 + Gd_2O_3 in the ratio 1:1.5:1 in cell 1; a mixture of Pd + Gd_2PdO_4 + Gd_4PdO_7 in the ratio 1:1.5:1 in cell 2; a mixture of Pd + $Gd_2Pd_2O_5$ + Gd_2PdO_4 in the ratio 1:1.5:1 in cell 3; a mixture of Pd + $Gd_2Pd_2O_5$ + Gd_4PdO_7 in the ratio 1:1.5:1 in cell 4. In each case, an excess of the component that decomposed to establish the oxygen pressure in the closed system was taken. The average particle size of the powders used to prepare the working and buffer electrodes was in the range from 3 to 8 μm.

The details of cell assembly and operational procedures used in this study were identical with those reported elsewhere [11,12]. At the end of each experiment, the electrodes were cooled to room temperature and examined by optical and scanning electron microscopy and XRPD. Although small changes in the relative concentration of the constituents were observed in some cases, the number and nature of the phases remained unaltered. The change in relative concentration was consistent with the expected decomposition of one of the oxides at high-temperature to generate the equilibrium oxygen pressure in sections of the apparatus.

Observed in preliminary experiments was cyclic fluctuation in emf at constant temperature; the magnitude was ±1.8 mV for cell 1. The resistance of the cell increased with time at 1300 K indicating the gradual formation of a non-conducting phase at the electrode/electrolyte interface. Careful examination of the interface using cross-sectional transmission electron microscopy (TEM) indicated localized islands of $Gd_2Zr_2O_7$. Physical contact of Gd_2O_3 in the electrode with the solid electrolyte was therefore avoided by coating the electrolyte surface with a thin layer of metal Pd. Painted on all surfaces of the solid electrolyte in contact with the working and buffer electrodes was a solution of $PdCl_2$. After firing in air at 1275 K, a thin film of Pd metal was obtained. The process was repeated three times to obtain a satisfactory coating on the whole contact surface. The Pd film on the electrolyte converts partly into tiny spheres when held at 1375 K for 2 h. With the introduction of the spherical Pd barrier at electrode/electrolyte interface, the fluctuation in emf decreased to ±0.2 mV. Hence, the Pd barrier was used in subsequent measurements on the different cells.

3. Results and discussion

3.1. Phase diagram

The isothermal section at 1223 K of the equilibrium phase diagram for the system Gd–Pd–O, composed from the results obtained by equilibration and phase identification of quenched samples by optical and scanning electron microscopy, EDS and XRPD, are shown in Fig. 1. Equilibrium was assumed when the XRPD or EDS showed no change after successive heat treatments. In several phase fields, equilibrium was confirmed by using different starting materials to produce samples of the same average chemical composition, and verifying that the samples had identical phase composition after equilibration. There was no difference in the phase composition of identical samples quenched into liquid nitrogen and chilled mercury.

Along the binary Pd–O, there was no stable oxide at 1223 K. Along the Gd–O binary, Gd_2O_3 was detected. A liquid phase was present along the Gd–Pd binary for $0.19 \leq X_{Pd} \leq 0.33$. Along the binary Gd–Pd, four intermetallics (GdPd, Gd_3Pd_4, $GdPd_2$ and '$GdPd_3$') and Pd-rich solid solution were observed in addition to the liquid phase. The compound '$GdPd_3$' is non-stoichiometric. These results are in general agreement with the phase diagram for Gd–Pd binary available in the literature [13]. All the three ternary oxides lie on the Gd_2O_3–PdO join. The ternary compounds were slightly non-stoichiometric, although their precise boundaries could not be established using EDS. The XRPD patterns of the oxides in different phase field were almost identical. The valence of Pd in all the oxides encountered in this study was two.

Metal Pd was found to be in equilibrium with Gd_2O_3 and the ternary oxide phases in different phase fields. Three three-phase fields involving Pd and the different ternary oxides were identified at 1223 K. Each of these phase fields involving three condensed phases is characterized by an unique oxygen potential at constant temperature and total pressure in accordance with the phase rule. Measurement of the oxygen partial pressure in the three-phase regions provides a means for determining the Gibbs energies of formation of the ternary oxides. Each of the three ternary oxides were stable in the presence of pure oxygen gas at 1223 K. The Gd–Pd liquid, inter-metallics and Pd-rich solid solution were found to be in equilibrium with Gd_2O_3.

3.2. Standard Gibbs energies of formation of ternary oxides

Polarization of the buffer electrode was small but significant in cells 1–4: the absolute value of the emf of the buffer electrode against the reference was 6–14 mV lower than that of the working electrode. The variation of the oxygen potential across the three electrode cell is shown in Fig. 3. The polarization effect (E_p) is given by:

$$E_p = E_{r/w} - E_{r/b} - E_{b/w} \quad (1)$$

where $E_{r/w}$ is the correct emf of the cell measured between the unpolarized reference and working electrodes, $E_{r/b}$ is the emf between the reference and buffer electrodes, and $E_{b/w}$ is the emf between the buffer and working electrodes. The emf across each solid electrolyte membrane is related to the oxygen potential difference across it. E_p is the electrochemical equivalent of the oxygen potential gradient across the buffer electrode. The polarization effect was more

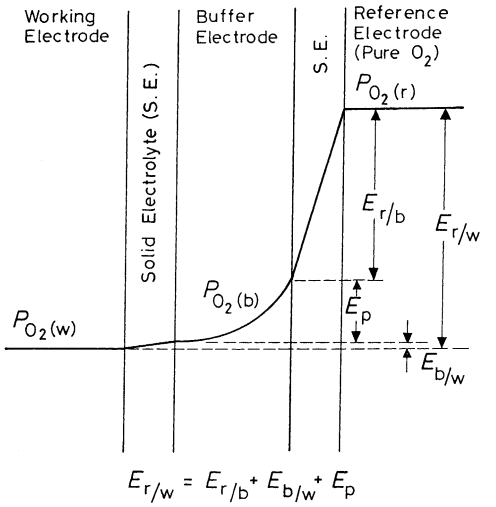

Fig. 3. The variation of the oxygen potential across the solid-state cell incorporating the buffer electrode. An exaggerated schematic of polarization of the buffer electrode is presented. A method of assessing the magnitude of the polarization effect from the electrical potential difference between the three electrodes is illustrated.

pronounced at high-temperatures. Thus, the need for the buffer electrode for accurate thermodynamic measurements was clearly demonstrated.

The reversible emfs of cells 1–4 are shown as a function of temperature in Fig. 4. The linear least-squares regression

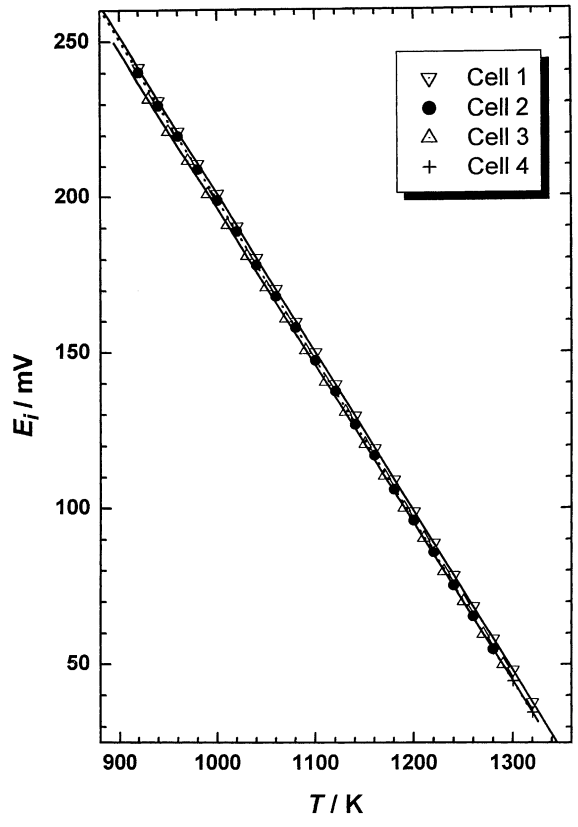

Fig. 4. The variation of the reversible emfs of cells 1–4 with temperature.

analysis of the emf of cell 1 in the temperature range from 920 to 1320 K gives,

$$E_1/\text{mV} = 709.7 - 0.5089T(\pm 0.34) \quad (2)$$

The uncertainty limit corresponds twice to the standard error estimate. The emf of cell 1 is related to the standard Gibbs energy of formation of Gd_4PdO_7 from Gd_2O_3, Pd and O_2 gas

$$2Gd_2O_3(s) + Pd(s) + 1/2O_2(g) \rightarrow Gd_4PdO_7(s) \quad (3)$$

$$\Delta_{r(3)}G^0/\text{J mol}^{-1} = -2FE_1 = -136,950 + 98.20T \quad (\pm 70) \quad (4)$$

where F is the Faraday constant and $\Delta_{r(3)}G^0$ represents the standard Gibbs energy change for reaction (3). Gd_2O_3 used in this study had the cubic structure (space group $Ia\bar{3}$). The standard Gibbs energy of formation of PdO was determined recently [11]. For the formation of PdO

$$Pd(s) + 1/2O_2(g) \rightarrow PdO(s) \quad (5)$$

$$\Delta_f G^0/\text{J mol}^{-1} = -111,920 + 97.87T \quad (\pm 120) \quad (6)$$

Hence, the Gibbs energy of formation of Gd_4PdO_7 from its component oxides can be obtained by combining Eqs. (4) and (6). For the reaction,

$$2Gd_2O_3(s, \text{C-Rare Earth}) + PdO(s) \rightarrow Gd_4PdO_7(s) \quad (7)$$

$$\Delta_{r(7)}G^0 = \Delta_{f(ox)}G^0(Gd_4PdO_7)/\text{J mol}^{-1} = -25,030 + 0.33T \quad (\pm 140) \quad (8)$$

The temperature-independent term on the right hand side of Eq. (8) is the enthalpy of formation of Gd_4PdO_7 from component oxides at an average temperature of ~1120 K. The temperature-dependent term is related to the corresponding entropy of formation.

The emf of cell 2 was reproducible and varied linearly with temperature in the range 920–1280 K. The least-squares regression analysis gives,

$$E_2/\text{mV} = 713.0 - 0.5141T \quad (\pm 0.44) \quad (9)$$

The emf of cell 2 is related to the standard Gibbs energy change for the reaction

$$Gd_4PdO_7(s) + Pd(s) + 1/2O_2(g) \rightarrow 2Gd_2PdO_4(s) \quad (10)$$

$$\Delta_{r(10)}G^0/\text{J mol}^{-1} = -2FE_2 = -137,590 + 99.21T \quad (\pm 85) \quad (11)$$

Combining reactions (3), (5), and (10), one obtains the reaction representing the formation of Gd_2PdO_4 from its component oxides

$$Gd_2O_3(s, \text{C-Rare Earth}) + PdO(s) \rightarrow Gd_2PdO_4(s) \quad (12)$$

$$\Delta_{r(12)}G^0 = \Delta_{f(ox)}G^0(Gd_2PdO_4)/J\ mol^{-1} = -25,350 + 0.84T \quad (\pm 135) \tag{13}$$

The measured emf of cell 3 can be expressed by the relation:

$$E_3/mV = 701.0 - 0.5048T \quad (\pm 0.5) \tag{14}$$

At higher temperatures, Gd_2PdO_4 was found to decompose gradually to a mixture of Gd_4PdO_7 and $Gd_2Pd_2O_5$. Thus, the solid-state decomposition temperature of Gd_2PdO_4 is 1280 K and this temperature should be independent of oxygen partial pressure. The emf of cell 3 is related to the standard Gibbs energy change for the reaction:

$$Gd_2PdO_4(s) + Pd(s) + 1/2O_2(g) \rightarrow Gd_2Pd_2O_5(s) \tag{15}$$

$$\Delta_{r(15)}G^0/J\ mol^{-1} = -2FE_3 = -135,270 + 97.41T \quad (\pm 100) \tag{16}$$

The standard Gibbs energy of formation of $Gd_2Pd_2O_5$ from its component oxides can be computed by combining the standard Gibbs energy changes associated with Eqs. (3), (5), (10) and (15);

$$Gd_2O_3(s, C\text{-Rare Earth}) + 2PdO(s) \rightarrow Gd_2Pd_2O_5(s) \tag{17}$$

$$\Delta_{r(17)}G^0 = \Delta_{f(ox)}G^0(Gd_2Pd_2O_5)/J\ mol^{-1} = -48,700 + 0.38T \quad (\pm 270) \tag{18}$$

Above 1280 K, a three-phase region involving Pd, Gd_4PdO_7 and $Gd_2Pd_2O_5$ was found to emerge. Cell 4 measured the oxygen potential in this three-phase field. The emf of cell 4 can be expressed by the relation:

$$E_4/mV = 704.5 - 0.5075T \quad (\pm 0.35) \tag{19}$$

The emf of cell 4 was obtained only in a limited temperature range from 1280 to 1320 K. The emf of cell 4 is related to the standard Gibbs energy change for the reaction:

$$Gd_4PdO_7(s) + 3Pd(s) + 3/2O_2(g) \rightarrow 2Gd_2Pd_2O_5(s) \tag{20}$$

$$\Delta_{r(20)}G^0/J\ mol^{-1} = -6FE_4 = -407,840 + 293.80T \quad (\pm 200) \tag{21}$$

This result can be independently calculated from the emfs of cells 2 and 3:

$$\Delta_{r(20)}G^0/J\ mol^{-1} = -2F(E_2 + 2E_3) = -408,130 + 294.03T \quad (\pm 210) \tag{22}$$

Both methods give almost identical results for the Gibbs energy in the temperature range of measurement. Although such good agreement may be fortuitous, it clearly demonstrates the internal consistency of the emf data.

The emf of cell 4 was identical to that of cells 2 (54.9 mV) at 1280 K. However, the values of the decomposition temperature of Gd_2PdO_4 obtained by solving the three equations for emf, in binary combinations, are slightly different. The emf of cells 2 and 3 intersect at 1290 K, cells 2 and 4 at 1288 K, and cells 3 and 4 at 1296 K.

Without the use of the buffer electrode, the measured emf would have been lower by 6–14 mV for each cell involving a three-phase electrode. Because of polarization, the measured Gibbs energies of formation would have been more positive. The reference electrode used in this study (pure O_2 at 0.1 MPa) is non-polarizable. When polarizable reference electrodes are used, it is necessary to introduce another buffer electrode with almost identical chemical potential adjacent to the reference. In the absence of a driving force, there would then be no oxygen flux through the solid electrolyte membrane separating the reference electrode and its buffer under open circuit conditions. Consequently, the reference electrode would be protected from polarization. Thus, polarization would be confined to the two buffer electrodes.

The dissociation temperature of the compounds in air computed from the thermodynamic data obtained in this study can be compared with values reported in the literature [2], which are probably associated with an uncertainty of 10–15 K. Table 1 indicates that the dissociation temperature of $Gd_2Pd_2O_5$ in air obtained from the results of this study is in good agreement with the values reported by McDaniel and Schneider [2]. The values for the solid-state decomposition temperature of Gd_2PdO_4 obtained in the two studies are also in fair agreement. McDaniel and Schneider [2] did not identify the compound Gd_4PdO_7. The literature does not contain any thermodynamic information on the ternary oxides for comparison with the results obtained in this study.

The Gibbs energy of mixing for the system Gd_2O_3–PdO at 1223 K is shown in Fig. 5 as a function of composition. The value of the Gibbs energy of mixing for each compound is obtained by dividing its standard molar Gibbs energy of formation from the component binary oxides by the number of molecules of the binary oxides present in the compound. The minimum in the Gibbs energy of mixing occurs at the 1:2 composition corresponding to the compound $Gd_2Pd_2O_5$. The enthalpy of mixing also has a similar shape since entropies of formation of all the ternary compounds from Gd_2O_3

Table 1
Dissociation temperatures of Gd_4PdO_7, $Gd_2Pd_2O_5$, and Gd_2PdO_4

Compound	Dissociation temperature (T, K)		Reference
	Air	O_2 (0.1 MPa)	
Gd_4PdO_7	1308 (±1)	1395 (±1)	This study
Gd_2PdO_4[a]	1278 (±15)	–	[2]
	1280 (±5)	1280 (±5)	This study
$Gd_2Pd_2O_5$	1298 (±10)	–	[2]
	1302 (±1)	1389 (±1)	This study

[a] Solid-state decomposition to Gd_4PdO_7 and $Gd_2Pd_2O_5$.

Table 2
The standard Gibbs energies of formation of Gd_2O_3, Gd_4PdO_7, Gd_2PdO_4, and $Gd_2Pd_2O_5$ from elements

Compound	$\Delta_f G^0$/J mol^{-1} (920–1320 *K*)
Gd_2O_3	$-1{,}815{,}850 + 276.24T$ ($\pm$4040)
Gd_4PdO_7	$-3{,}768{,}650 + 650.68T$ ($\pm$8080)
Gd_2PdO_4	$-1{,}953{,}120 + 374.95T$ ($\pm$4040)
$Gd_2Pd_2O_5$	$-2{,}088{,}390 + 472.36T$ ($\pm$4040)

and PdO are numerically small and have the same sign. All the ternary oxides are primarily stabilized by their large negative enthalpies of formation.

The standard Gibbs energy of formation of the ternary oxides from elements can be readily calculated as a function of temperature in the range $920 \leq T \leq 1320$ K using the results obtained in this study and values for the Gibbs energy of formation of cubic Gd_2O_3 from the compilation of Pankratz [14]. The calculated values are given in Table 2 along with the standard Gibbs energy of Gd_2O_3. For each compound, the data are represented by linear equations. Using the Neumann–Kopp rule to estimate the heat capacity of the ternary oxides relative to their constituent binary oxides, thermodynamic properties of the ternary oxides at 298.15 K can be evaluated. The standard enthalpies and entropies of formation of the three inter-oxide compounds from component binary oxides and from elements, and their standard entropies are listed in Table 3. The thermodynamic data for Gd ($S^0_{298.15}$/J mol^{-1} K^{-1} = 67.95), O_2 ($S^0_{298.15}$/J mol^{-1} K^{-1} = 205.037), Pd ($S^0_{298.15}$/J mol^{-1} K^{-1} = 37.71) and Gd_2O_3 ($S^0_{298.15}$/J mol^{-1} K^{-1} = 150.624; $\Delta H^0_{298.15}$/kJ mol^{-1} = −1826.9) from Pankratz [14], and PdO ($S^0_{298.15}$/J mol^{-1} K^{-1} = 37.25; $\Delta H^0_{298.15}$/kJ mol^{-1} = −115.51) obtained from Ref. [11] were used.

3.3. Chemical potential diagrams

The oxygen chemical potential diagram for the system Gd–Pd–O at 1223 K, computed from the results of this study is shown in Fig. 6. The composition variable is cationic fraction, $\eta_{Pd}/(\eta_{Gd} + \eta_{Pd})$, where η_i represents moles of component *i*. Since oxygen is not included in the composition parameter, information on oxygen non-stoichiometry cannot be displayed on the diagram. Nevertheless, the diagram provides useful information on the oxygen potential range for the stability of the various phases. The diagram is complimentary to the conventional Gibbs triangle representation of phase relations in ternary systems (see Fig. 1 as an example), where the composition of each phase can be unambiguously displayed. All the topological rules of construction for conventional temperature-composition phase diagrams are applicable to the oxygen potential diagram shown in Fig. 6.

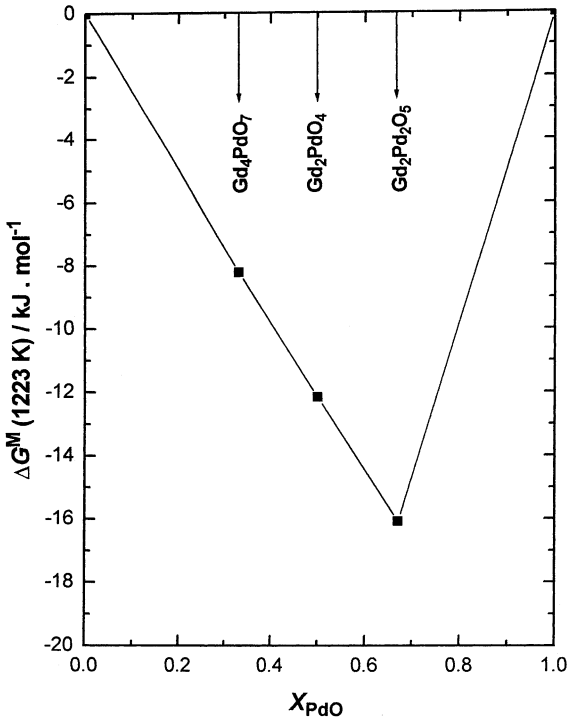

Fig. 5. The Gibbs energy of mixing as a function of composition for the pseudo-binary system Gd_2O_3–PdO at 1223 K.

When three condensed phases coexist at equilibrium in a ternary system such as Gd–Pd–O, the system is bivariant; at a fixed temperature and total pressure, three condensed phases coexist only at a unique partial pressure of oxygen. Therefore, horizontal lines on the diagram represent three-phase equilibria. On reducing the oxygen partial pressure at 1223 K, $Gd_2Pd_2O_5$ dissociates first at $(P_{O2}/P^0) = -1.378$, where $P^0 = 0.1$ MPa is the standard atmospheric pressure. This is followed by the decomposition of Gd_2PdO_4 at a slightly reduced pressure, $(P_{O2}/P^0) = -1.389$. The compound Gd_4PdO_7 is the last ternary oxide to decompose $(P_{O2}/P^0) = -1.439$ on reducing the oxygen partial pressure. The oxygen potentials corresponding to the equilibria between alloys/inter-metallics and the gadolinium sesquioxide are computed using data for the oxide Gd_2O_3 from Pankratz [14] and estimated data for Gd–Pd alloys, which are listed in Tables 2 and 4, respectively. The estimated data

Table 3
Thermodynamic properties of Gd_4PdO_7, Gd_2PdO_4 and $Gd_2Pd_2O_5$ at 298.15 K

Compound	$\Delta_{f(ox)}H^0_{298.15}$ kJ mol^{-1}	$\Delta_f H^0_{298.15}$ kJ mol^{-1}	$\Delta_{f(ox)}S^0_{298.15}$J mol^{-1} K^{-1}	$\Delta_f S^0_{298.15}$J mol^{-1} K^{-1}	$S^0_{298.15}$J mol^{-1} K^{-1}
Gd_4PdO_7	−25.03 ($\pm$0.48)	−3794.34 ($\pm$10.01)	−0.33 ($\pm$0.48)	−689.14 ($\pm$1.78)	338.17 ($\pm$0.87)
Gd_2PdO_4	−25.35 ($\pm$0.48)	−1967.76 ($\pm$5.02)	−0.84 ($\pm$0.47)	−396.82 ($\pm$0.99)	187.04 ($\pm$0.69)
$Gd_2Pd_2O_5$	−48.70 ($\pm$0.96)	−2106.62 ($\pm$5.10)	−0.38 ($\pm$0.96)	−499.51 ($\pm$1.31)	224.75 ($\pm$1.29)

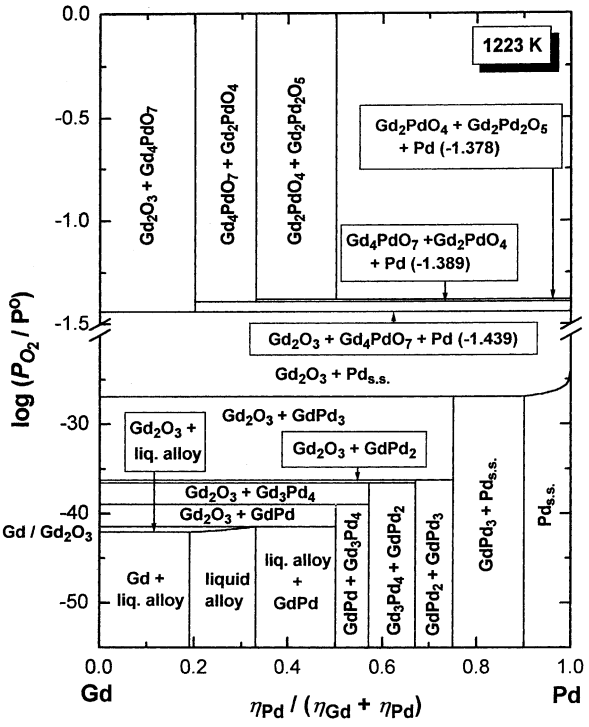

Fig. 6. Oxygen potential diagram for the system Gd–Pd–O at 1223 K.

for the Gd–Pd alloys were based primarily on calorimetric data of Guo and Kleppa [15], adjusted for consistency with phase relations obtained in this study. Similar oxygen potential diagrams at other temperatures, that may be required to address specific applications, can be readily computed from the thermodynamic data. Phase relations can also be computed as a function of temperature at constant oxygen partial pressure; plots for $(P_{O2}/P^0) = 1.0$ *and* 0.21 are shown in Fig. 7(a) and (b), respectively. It is apparent that the phase diagram is very sensitive to the partial pressure of oxygen.

It is interesting to view the stability of the various phases as a function of the chemical potentials of the three components. A three-dimensional representation at 1223 K is displayed in Fig. 8(a). The stability domain of each stoichiometric phase is defined by a plane, because the sum of the chemical potentials of the different components weighted by the appropriate stoichiometric coefficients is equal to the Gibbs energy of formation of the phase. Since the Gibbs energies of the alloy phases are functions of composition, they appear as a curved surfaces on the diagram. The stability of Gd_2PdO_4 and Gd_4PdO_7 are very restricted at 1223 K. In Fig. 8(a), the phases are represented as lines (planes with almost zero width). An expanded view with a little better resolution of stability domain of Gd_2PdO_4 and Gd_4PdO_7 is

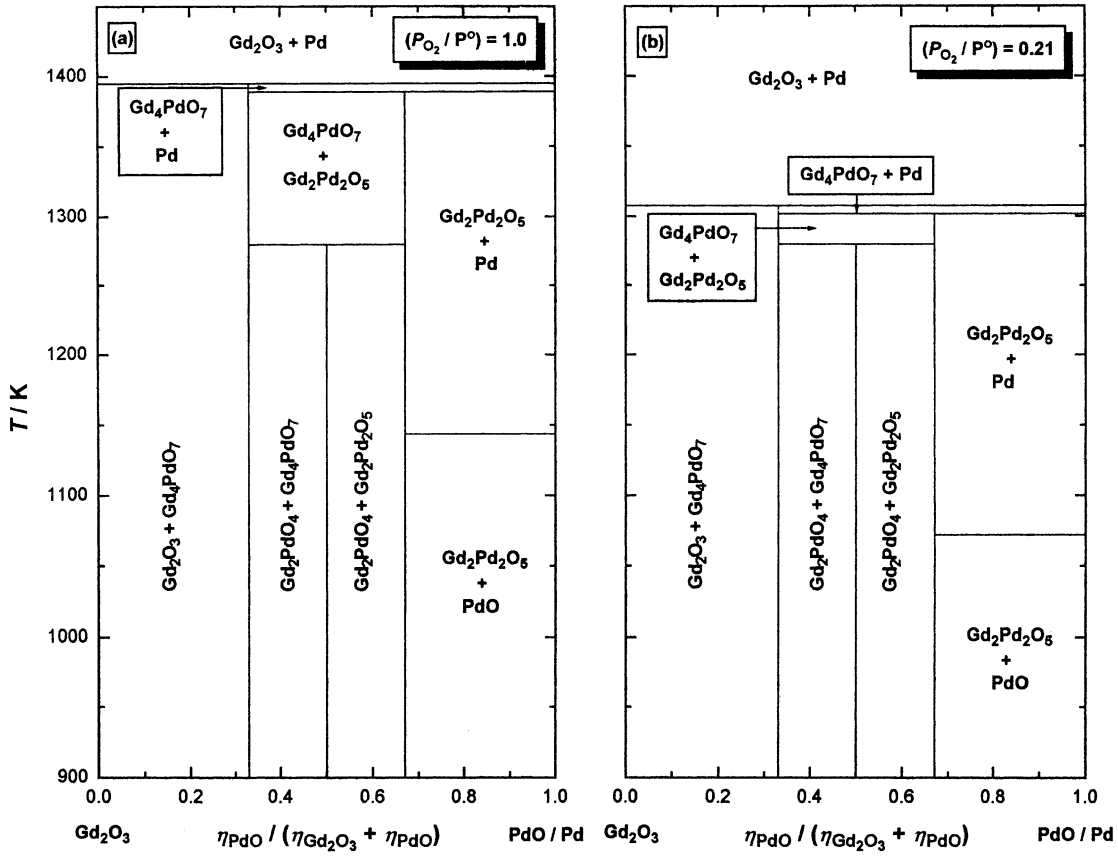

Fig. 7. Isobaric phase diagrams for the system Gd–Pd–O: (a) $(P_{O2}/P^0) = 1.0$ and (b) $(P_{O2}/P^0) = 0.21$, where P^0 is the standard atmospheric pressure (0.1 MPa).

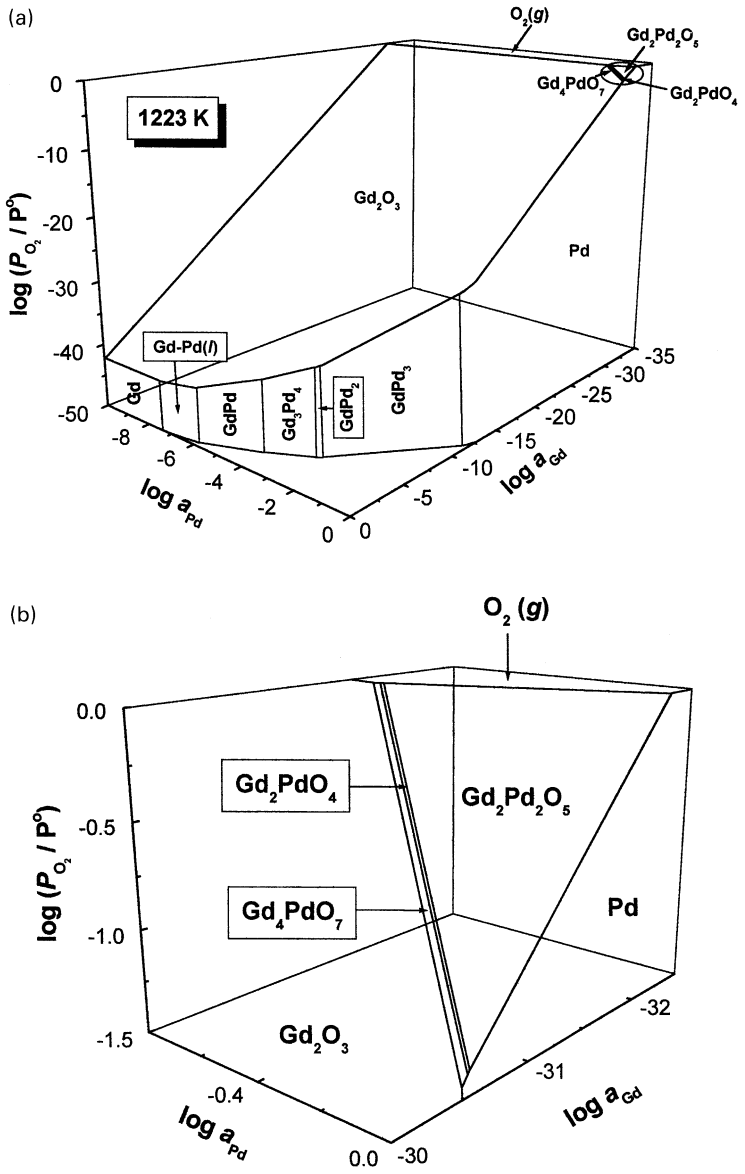

Fig. 8. (a) Three-dimensional chemical potential diagram for the system Gd–Pd–O at 1223 K. Surfaces represent the stability domains of the various condensed phases as a function of the chemical potentials of the three components. (b) An expanded view of stability region of ternary oxides.

Table 4
Thermodynamic data for the system Gd–Pd

Phase	Gibbs energy of mixing, ΔG^M/J.(g at)$^{-1}$	Reference states
GdPd	$-77{,}365 + 1.18T$	Solid Pd, Gd
Gd_3Pd_4	$-83{,}150 + 3.48T$	Solid Pd, Gd
$GdPd_2$	$-86{,}065 + 7.94T$	Solid Pd, Gd
$GdPd_3$	$-79{,}700 + 5.47T$	Solid Pd, Gd
Liquid alloy	$RT\sum_{i=\mathrm{Gd,Pd}} X_i \ln X_i - X_{Gd}X_{Pd}(160{,}000X_{Gd} + 375{,}000X_{Pd})$	Liquid Pd, Gd
Solid solution (Pd-rich)	$RT\sum_{i=\mathrm{Gd,Pd}} X_i \ln X_i - X_{Gd}X_{Pd}(120{,}000X_{Gd} + 350{,}000X_{Pd})$	Solid Pd, Gd

displayed in Fig. 8(b). Lines, defined by the intersection of the planes or surfaces, represent two-phase fields. Points of intersection of three planes or surfaces identify three-phase equilibria. It is seen that the stability domains of the ternary oxides are restricted to the top right corner of the diagram, where the activity of Pd and the partial pressure of oxygen have relatively large values and the activity of Gd is very low. In reducing atmospheres Gd_4PdO_7 with decompose to nanocrystalline Pd on microcrystalline Gd_2O_3 as reported by Andersson et al. [1]. The nanocrystalline Pd can act as a three-way catalyst for the conversion of CO, NO, and propene simultaneously to CO_2, N_2 and H_2O [16]. The ternary oxide has two roles: it functions as the precursor for in situ generation of nanocrystalline Pd on Gd_2O_3, and as the oxidation product that can easily regenerate the

catalyst in finely divided form by heat treatment in reducing atmospheres.

4. Conclusions

Isothermal section of the phase diagram of the system Gd–Pd–O at 1223 K has been established by phase analysis of samples quenched after equilibration at high-temperature. Three ternary oxides, Gd_4PdO_7, Gd_2PdO_4 and $Gd_2Pd_2O_5$ were found to be stable. Based on the phase diagram, three solid-state cells were designed to measure the chemical potential of oxygen corresponding to three separate phase fields in the ternary, each involving three condensed phases. During the course of the measurements, it was found that Gd_2PdO_4 decomposes to Gd_4PdO_7 and $Gd_2Pd_2O_5$ at 1280 K. Hence a fourth cell was designed to measure the oxygen potential in the three-phase field Pd + Gd_4PdO_7 + $Gd_2Pd_2O_5$. The emf measurements were conducted from 920 to 1320 K against the primary reference standard for oxygen potential. The advanced design of the solid-state cell used in this study incorporating a buffer electrode was used. Introducing a thin layer of Pd in spherical form at the electrode/electrolyte interface minimized interaction between Gd_2O_3 and (Y_2O_3) ZrO_2 electrolyte. These novel features enhanced the accuracy of thermodynamic data. The Gibbs energy changes corresponding to the following reactions were directly measured:

$$2Gd_2O_3(s, \text{C-Rare Earth}) + Pd(s) + 1/2O_2(g) \rightarrow Gd_4PdO_7(s)$$

$$\Delta_r G^0/\text{J mol}^{-1} = -136,950 + 98.20T \qquad (\pm 70)$$

$$Gd_4PdO_7(s) + Pd(s) + 1/2O_2(g) \rightarrow 2Gd_2PdO_4(s)$$

$$\Delta_r G^0/\text{J mol}^{-1} = -137,590 + 99.21T \qquad (\pm 85)$$

$$Gd_2PdO_4(s) + Pd(s) + 1/2O_2(g) \rightarrow Gd_2Pd_2O_5(s)$$

$$\Delta_r G^0/\text{J mol}^{-1} = -135,270 + 97.41T \qquad (\pm 100)$$

$$Gd_4PdO_7(s) + 3Pd(s) + 3/2O_2(g) \rightarrow 2Gd_2Pd_2O_5(s)$$

$$\Delta_r G^0/\text{J mol}^{-1} = -407,840 + 293.80T \qquad (\pm 200)$$

From accurate measurements on cells incorporating buffer electrodes, the Gibbs energies, enthalpies and entropies of formation of the ternary oxides Gd_4PdO_7, $Gd_2Pd_2O_5$, and Gd_2PdO_4 were deduced for the first time. Chemical potential diagrams including a three-dimensional representation for the system Gd–Pd–O at 1223 K were developed based on the thermodynamic data obtained in this study and auxiliary information from the literature.

Acknowledgements

One of the authors (Kay Thi Lwin) is grateful to the Indian Council for Cultural Relations (ICCR) for financial assistance.

References

[1] M. Andersson, E. Bakchinova, K. Jansson, M. Nygren, J. Mater. Chem. 9 (1999) 265.
[2] C.L. McDaniel, S.J. Schneider, J. Res. Natl. Bur. Stand. A 72 (1968) 27.
[3] M. Andersson, J. Grins, M. Nygren, J. Solid State Chem. 146 (1999) 428.
[4] J.N. Pratt, Metall. Trans. A 21 (1990) 1223.
[5] J. Fouletier, P. Fabry, M. Kleitz, J. Electrochem. Soc. 123 (1976) 204.
[6] P. Villars, L.D. Calvert, Pearson's Handbook of Crystallographic Data for Intermetallic Phases, 2nd ed, vol. 3, 1991, p. 3633.
[7] K.T. Jacob, T. Mathews, J. Mater. Chem. 1 (1991) 545.
[8] K.T. Jacob, J.H.E. Jeffes, Trans. Inst. Min. Metall. Sec. C80 (1971) C181.
[9] G.G. Charette, S.N. Flengas, J. Electrochem. Soc. 115 (1968) 796.
[10] G.M. Kale, K.T. Jacob, Metall. Trans. B 23 (1992) 57.
[11] K.T. Jacob, T.H. Okabe, T. Uda, Y. Waseda, J. Phase, Equilibria 20 (1999) 553.
[12] K.T. Jacob, T.H. Okabe, T. Uda, Y. Waseda, Mater. Sci. Engng B64 (1999) 44.
[13] T.B. Massalski, P.R. Subramanian, H. Okamoto, L. Kacprzak (Eds.), second ed, Binary Alloy Phase Diagrams, vol. 3, ASM International, Materials Park, Ohio, 1990, p. 1909.
[14] L.B. Pankratz, Thermodynamic properties of elements and oxides, Bulletin 672, United States Bureau of Mines, 1982.
[15] Q. Guo, O.J. Kleppa, J. Alloy Compd 221 (1995) 45.
[16] M. Andersson, K. Jansson, M. Nygren, Catal. Lett. 39 (1996) 253.